Laser postionization secondary neutral mass spectrometry in tissue: a powerful tool for elemental and molecular imaging in the development of targeted drugs

Andrea Wittig,[1] Heinrich F. Arlinghaus,[3] Christian Kriegeskotte,[3] Raymond L. Moss,[4] Klaas Appelman,[5] Kurt W. Schmid,[2] and Wolfgang A.G. Sauerwein[1]

[1]Department of Radiation Oncology and [2]Institute for Pathology and Neuropathology, University Duisburg-Essen, University Hospital Essen, Essen, Germany; [3]Physikalisches Institut, Westfälische Wilhelms-Universität Münster, Münster, Germany; [4]HFR Unit, Institute for Energy, Joint Research Centre, European Commission; and [5]Nuclear Research and Consultancy Group, NRG, Petten, The Netherlands

Abstract

The exact intracellular localization and distribution of molecules and elements becomes increasingly important for the development of targeted therapies and contrast agents. We show that laser postionization secondary neutral mass spectrometry (laser-SNMS) is well suited to localize particular elements and small molecules with subcellular spatial resolution applying the technique exemplary to Boron Neutron Capture Therapy (BNCT). We showed in a murine sarcoma that the drugs used for clinical BNCT, namely L-*para*-boronophenylalanine (700 mg/kg body weight i.p.) and sodium mercaptoundecahydro-*closo*-dodecaborate (200 mg/kg body weight i.p.), transport the therapeutic agent ^{10}B into the cytoplasm and into the nucleus itself, the most sensitive area of the cell. Sodium mercaptoundecahydro-*closo*-dodecaborate distributes ^{10}B homogeneously and L-*para*-boronophenylalanine heterogeneously. When combining laser-SNMS with prompt γ-ray analysis as a screening technique, strategies for BNCT can be elaborated to develop new drugs or to improve the use of existing drugs on scientifically based evidence. The study shows the power of laser-SNMS in the early stages of drug development, also outside BNCT. [Mol Cancer Ther 2008;7(7):1763–71]

Received 3/3/08; accepted 4/30/08.

Grant support: European Commission contract QLK3-CT-1999-01067 (FP5) and contract 005045 (FP6).

The costs of publication of this article were defrayed in part by the payment of page charges. This article must therefore be hereby marked *advertisement* in accordance with 18 U.S.C. Section 1734 solely to indicate this fact.

Requests for reprints: Andrea Wittig, Department of Radiation Oncology, University Duisburg-Essen, University Hospital Essen, Hufelandstrasse 55, 45122 Essen, Germany. Phone: 49-201-723-2050; Fax: 49-201-723-5908. E-mail: andrea.wittig@uni-due.de

doi:10.1158/1535-7163.MCT-08-0191

Introduction

Imaging of elements and molecules with subcellular spatial resolution becomes increasingly important in the development of modern therapeutic and diagnostic strategies in medicine. Such strategies rely on the capability of specialized compounds to selectively target specific cells. The application of imaging techniques, such as mass spectrometry, provides an excellent tool to guide decisions already in the initial stages of drug development. Laser postionization secondary neutral mass spectrometry (laser-SNMS) can simultaneously detect atoms, their isotopes and molecules (through well defined small fragments), in tissue with high sensitivity and with microscopic spatial resolution (1). The principal advantage of this technology is the ability to directly observe the distribution of elements and molecules without specific labeling by fluorescent or radioactive probes. Laser-SNMS seems to particularly provide benefit for drug testing in Boron Neutron Capture Therapy (BNCT). BNCT is a biologically targeted form of radiotherapy, which uses the ability of the isotope ^{10}B to capture thermal neutrons leading to the nuclear reaction $^{10}B(n,\alpha,\gamma)^{7}Li$. This reaction produces 478 keV γ-rays, ^{4}He and ^{7}Li particles. The latter two have high linear energy transfer properties and therefore a high biological effectiveness relative to conventional photon irradiation. The range of these particles in tissue is limited to ~10 μm, which confines their effect to one cell diameter, thus providing the potential for a targeted irradiation of tumor cells.

^{10}B-containing compounds used for BNCT do not have any therapeutic effect by themselves. As a consequence, conventional methods to test the efficacy of candidate drugs are not applicable. However, data on the macroscopic ^{10}B concentration and the microscopic ^{10}B distribution in tumors and surrounding healthy tissues are prerequisites to identify ^{10}B compounds, which selectively target specific tumor types. Quantitative approaches, such as prompt γ-ray analysis (PGRA), can reliably yield average ^{10}B concentrations to within 1 ppm from gross tissue specimens (2). Sample volumes, however, that can be measured with these methods are much larger than the volume irradiated by the $^{10}B(n,\alpha)^{7}Li$ reaction. In BNCT, the clinical efficacy of the therapy is substantially increased if the ^{10}B atoms are positioned close to a sensitive structure (the cell nucleus). Therefore, the ability to image the ^{10}B distribution in individual cells helps both in judging the potential of a certain drug in a given specific tumor type and in the understanding of underlying mechanisms of selectivity.

This study evaluates the potential of laser-SNMS in assessing the microscopic ^{10}B distribution in tissue samples.

The subcellular distribution of ^{10}B, using the two experimental compounds available for clinical BNCT, namely L-*para*-boronophenylalanine (BPA; ref. 3) and sodium mercaptoundecahydro-*closo*-dodecaborate (BSH; ref. 4), was compared. The second objective was to combine the information gained from laser-SNMS and PGRA using the same samples to evaluate if the two compounds BSH and BPA selectively accumulate in soft-tissue sarcoma offering a treatment option for this tumor type. The macroscopic ^{10}B concentration in a murine tumor model was compared with the ^{10}B concentration in the clinically relevant normal tissues, which might be dose limiting.

Materials and Methods

Animals and Tumors

Six- to 9-week-old male nude mice (HsdCpb:NMRI-*nu/nu*, kept at the Central Animal Facility of the University Hospital, Duisburg-Essen) were used for experiments. The health status of the mice was investigated quarterly in accordance with the recommendations of the Federation of European Laboratory Animal Science Associations (5). Animals had unlimited access to water and a high calorific nude mouse diet (12 ZH 10, Altromin). The experiments were authorized by the regulatory authority under TSG 683-02.

The histologic investigation of the MuEs tumor showed a tumor composed almost exclusively of spindle cells, which showed an infiltrative growth to adjacent nonneoplastic tissues. The tumors developed variably amounts of necrotic areas. Abundant mitoses were present. The vasculature within the tumors was thin-walled and usually dilated. The PAS reaction and AB-PAS reaction were negative as well as the immunohistochemical staining reactions for p53, epitope Ki-67 (MIB-1), and epithelial cytokeratin (LU-5). The tumor doubling time was 3 days. Tumor chunks of 2 to 3 mm were transplanted s.c. in the chest wall of anaesthetized mice. ^{10}B uptake studies were done on tumors with a diameter of 10 to 15 mm.

Boron Compounds

BSH ($Na_2^{10}B_{12}H_{11}SH$) was designed by Soloway et al. (4) to treat brain tumors. It was investigated clinically in malignant glioma (6, 7) and glioblastoma multiforme (European Organisation for Research and Treatment of Cancer 11961; refs. 8, 9). BPA ($C_9H_{12}{}^{10}BNO_4$) is a derivative of the neutral amino acid phenylalanine (3). It was used in clinical trials to treat glioblastoma and melanoma (10–12) and in combination with BSH to treat squamous cell carcinoma of head and neck (13, 14).

The systematic quality control of BSH and BPA (Katchem) and the preparation of injection solutions were done according to standard operating procedures established for the clinical BNCT trials of the European Organisation for Research and Treatment of Cancer (trials 11961, 11001, and 11011; refs. 8, 15, 16).

In keeping with the time range reported to be optimal in murine models (17–19), samples were collected 1.5 h after i.p. BPA injection (700 mg/kg) and 2.5 h after i.p. BSH injection (200 mg/kg). These doses correspond to twice the dose, which is used in the treatment protocols of the European Organisation for Research and Treatment of Cancer. One group of animals received either BSH or BPA; a third group received both drugs sequentially. Control animals were injected with saline following the same schedule.

Sample Preparation and Analysis with PGRS

Samples were taken with the animals deeply anaesthetized. Blood samples were taken by intracardial cannulation. Then, tumors, samples of skin, muscle, bone, and fat were removed. The samples were immediately weighed and stored in airtight containers at −20°C. The ^{10}B concentration in tissue or blood was analyzed by PGRA at the High Flux Reactor HFR Petten. PGRA measures the integral ^{10}B concentration in the sample volume by quantification of the 478 keV photon emission during the $^{10}B(n,\alpha,\gamma)^7Li$ reaction (2). Measurements were cross-calibrated with inductively coupled plasma-atomic emission spectroscopy. The minimum number of animals per data point was 4. The Kruskal-Wallis test was used to test for the global differences between treatments and the Wilcoxon test to compare each treatment group using SAS Software. P values < 0.05 were considered to prove statistical significance.

Sample Preparation and Analysis with Laser-SNMS

The feasibility of laser-SNMS in tissues depends on special cryopreparation techniques to preserve the chemical and structural integrity of living cells. Moreover, samples must withstand ion beam bombardment and high vacuum in the analysis chamber. Besides minimizing the time between tissue excision and sample freezing, it is important to maximize the cooling rate during the freezing process. A dedicated cryogenic sample preparation technique with a high cooling rate was validated for tissue samples (20, 21). Liquid propane was cooled below its boiling temperature using liquid nitrogen, thus accelerating the cooling process and preventing evaporation of propane at the contact surface of the immersed specimen. This allowed cooling rates of up to 10^4 K/s on the surface of the sample. Samples were prepared on conducting support material to prevent charging of the sample during ion bombardment (22). Small pieces of tissue (<1 mm^3) were placed on gold specimen carriers (Baltec) and shot into the liquid propane at high velocity. A slice of tissue was sectioned off from each block (Leika UCT ultramicrotome) at 193 K to remove damaged cells and contamination resulting from sample manipulation. The remaining block was freeze dried at a temperature of 193 K and a pressure of <1 Pa and stored under dry atmosphere. The face of the freeze-dried block was analyzed.

A combined gridless reflectron-based cryolaser-SNMS/TOF-secondary ion mass spectrometry (SIMS) instrument was used for the mass spectrometry analysis. Samples were bombarded with a pulsed 30 keV Ga^+ liquid metal ion gun (dc current: 1.4 nA) with a beam diameter of ~200 nm (total ion dose density: 1×10^{13}–1×10^{15} cm^{-2}). A focused excimer laser beam (λ = 193 nm, repetition rate: 200 Hz, pulse width: 10 ns, pulse energy: 100 mJ, and spot size

Table 1. Variation in mean ± SD absolute ^{10}B concentration and mean ± SD ^{10}B concentration ratio between tumor/blood and tumor/healthy tissues following an injection of BPA (700 mg/kg, 1.5 h before tissue sampling) or BSH (200 mg/kg, 2.5 h before tissue sampling) or both compounds sequentially

	Absolute ^{10}B concentration (ppm)		
	BSH	BPA	BSH + BPA
Tumor	14.9 ± 4.7	31.3 ± 4.0	36.6 ± 11.1
Blood	20.6 ± 8.0	13.9 ± 2.5	31.1 ± 11.1
Skin	8.4 ± 2.5	14.6 ± 3.2	20.11 ± 8.2
Muscle	2.2 ± 1.3	12.9 ± 1.8	13.2 ± 4.0
Bone	6.5 ± 1.3	7.5 ± 1.1	16.7 ± 1.1
Fat	1.5 ± 1.2	3.8 ± 1.3	3.6 ± 2.0
	^{10}B concentration ratio		
	BSH	BPA	BSH + BPA
Tumor/blood	0.7 ± 0.1	2.3 ± 0.5	1.3 ± 0.5
Tumor/skin	1.7 ± 0.4	2.3 ± 0.3	1.8 ± 0.4
Tumor/muscle	8.3 ± 3.2	2.5 ± 0.4	2.9 ± 0.6
Tumor/bone	2.6 ± 0.4	4.4 ± 1.1	1.9 ± 0.8
Tumor/fat	12.1 ± 4.1	8.8 ± 3.2	11.8 ± 5.4

diameter: 150 μm) was used to photoionize sputtered neutral particles. Laser-SNMS spectra were recorded with TOF-SIMS Software V3.12 (Ion-TOF) by scanning the primary ion beam over the analysis area, acquiring at each position mass spectra of the postionized secondary neutrals. For imaging of the lateral distribution of atoms and molecules, the intensities of the mass peaks in the spectra were calculated for each pixel of the rastered sample area and visualized with an intensity scale. The recorded data allow for imaging the distribution of every peak in the mass range of the analysis.

Ion-induced electron images were acquired from all samples by detecting the electrons produced by the scanning primary ion beam to select regions of interest for further analysis and to check the topography of the sample surface (1, 21). For each region of analysis, ion images for K, Na, P, Ca, ^{10}B, and additional molecular fragments were acquired. The chemical integrity of cells was verified by imaging and quantifying the K and Na distributions (23, 24). Preparation artifacts such as cell shrinkage and damage to cellular morphology usually common to freeze-dried samples were monitored with optical microscopy.

Results

^{10}B Concentrations in Tumors Measured with PGRA

The lowest mean ^{10}B concentration in the sarcoma was observed after BSH injection (Table 1). After BPA injection, the ^{10}B concentration was intermediate. The subsequent injection of BSH and BPA led to the highest ^{10}B concentration in the sarcoma. The increase was little below additive (Table 1). The amount of ^{10}B delivered by 200 mg BSH/kg body weight is higher (113.18 mg ^{10}B/kg) compared with 700 mg BPA/kg body weight (33.36 mg ^{10}B/kg), which has to be considered when the absolute ^{10}B concentrations are compared. The ^{10}B concentration ratio between tumor/blood after BSH injection was significantly lower compared with a BPA injection ($P < 0.01$). The ^{10}B concentration ratio between tumor/blood after a sequential injection of BSH and BPA was significantly lower compared with a single BPA injection ($P < 0.01$) but significantly higher than after BSH injection ($P < 0.01$) (Fig. 1).

The ^{10}B concentration ratios of tumor/healthy tissues are depicted in Fig. 2. The ^{10}B concentration ratio tumor/skin was not significantly different after BSH, BPA, or an injection of both compounds. The highest ^{10}B concentration ratios were found between tumor and fat; however, the ratios were not statistically different after an injection of BSH, BPA or both compounds. In contrast to these results, the ^{10}B ratio tumor/muscle was more favorable for the drug BSH as the ^{10}B concentration ratio was significantly higher after BSH compared with the injection of BPA or both compounds ($P < 0.01$). The ratio was not statistically different after injection of BPA or BPA + BSH ($P = 0.088$). The ^{10}B concentration ratio tumor/bone was significantly higher after BPA injection compared with BSH injection ($P < 0.01$) and injection of BSH + BPA ($P < 0.01$). The ratio did not significantly differ after BSH injection compared with BSH + BPA ($P = 0.11$).

Analysis of Boron Distribution with Laser-SNMS

In Figs. 3–5, the localization of specific ions and small molecules in tumor samples is shown. The ^{10}B distribution, as analyzed with laser-SNMS, was colocalized with specific cellular structures. These structures were identified by imaging the distribution of index molecules, which represent particular cell contents. For example, phosphorous is a constituent of polar head groups of phospholipids in lipids, proteins, and DNA. As such, the phosphorous signal is higher inside cells and thus can be used to identify

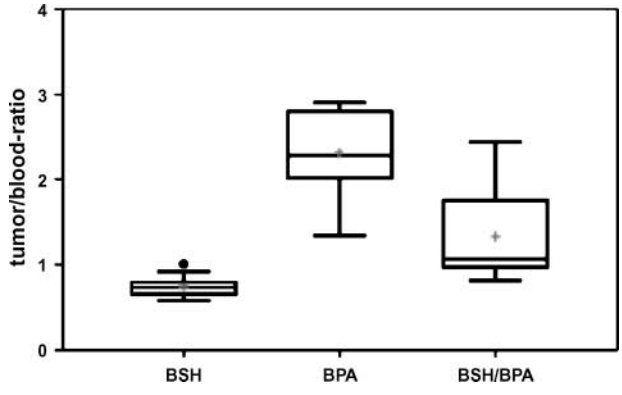

Figure 1. Variation of mean ± SD ^{10}B concentration ratios tumor/blood as measured with PGRA after i.p. injection of either BSH (200 mg/kg body weight 2.5 h before tissue sampling) or BPA (700 mg/kg body weight 1.5 h before tissue sampling) or a sequential injection of both compounds.

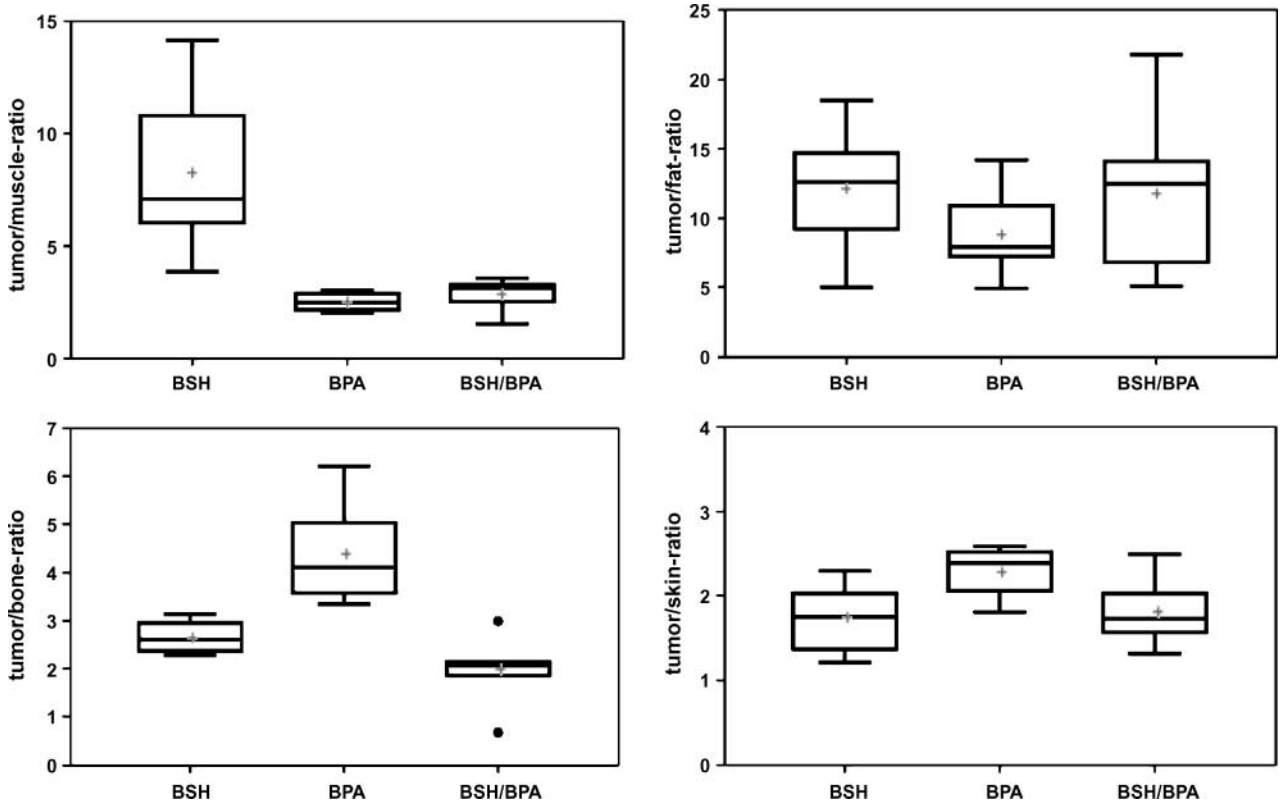

Figure 2. Variation of mean ± SD ^{10}B concentration ratios tumor/healthy tissues as measured with PGRA after i.p. injection of either BSH (200 mg/kg body weight 2.5 h before tissue sampling) or BPA (700 mg/kg body weight 1.5 h before tissue sampling) or a sequential injection of both compounds.

cells and cell boundaries. Earlier studies on membrane model systems have shown that C_3H_8N is a typical fragment of the quaternary amino group in the cholin head groups of lipids like phosphocholin and sphingomyelin (24, 25). This molecule was therefore used to identify membrane systems—not only the plasma membrane but also membrane layers surrounding cell organelles. CN is a small fragment, which is a constituent of many molecules, especially proteins and nucleic acids. It is thus found over the entire cellular area (26). Furthermore, the bases purine and pyrimidine in the DNA contain many CN bindings. A high contrast was observed in the pattern of CN with spots of much higher intensity with a diameter of ~5 to 7 μm in some intracellular areas (Figs. 3–5). In these areas, the C_3H_8N signal was low. It is likely that the nucleic membrane was removed in these areas by the fracturing process, leaving behind an open nucleus.

The ^{10}B image of the tumor treated with BSH (Fig. 3) shows a quite homogeneous distribution of the ^{10}B signal over the entire sample. Specific colors for each type of ion (red for CN, green for C_3H_8N, and blue for ^{10}B) were used for the superimposition of various ion images. This colocalization shows that the ^{10}B signal is clearly present in areas where also an intense C_3H_8N signal is present but also in areas with an intense CN signal. Within an individual laser-SNMS image, the level of brightness is directly proportional to the signal intensity. The ^{10}B signal is almost equally high in extracellular areas and within the cells in the cytoplasm and shows a quite homogeneous distribution.

In Fig. 4, ion images are shown from the MuEs sarcoma treated with BPA. Clearly, in this sample, the ^{10}B signal is not homogenously distributed but shows distinct differences between cells and inside single cells. ^{10}B signals are present within the cytoplasm and within the cell nucleus. However, there are no regions within the cells in which the ^{10}B signal is especially high and therefore suggesting one particular binding site.

A similar picture was observed in tumor samples of mice injected with both BSH and BPA (Fig. 5). The ^{10}B signal was not homogenously distributed and had varying intensities within single cells and within the tissue. Clearly, ^{10}B signals were again colocalized with areas of high intensity of the CN signal and the C_3H_8N signal. Obviously, it was not possible to distinguish whether a specific ^{10}B atom was delivered by BSH or BPA. This might be investigated by using, for example, ^{10}B for BPA and ^{11}B for BSH in future experiments.

Discussion

Precise knowledge of the distribution of a drug in tissues with subcellular resolution is not only regarded as crucial

for the development of drugs for targeted therapies, contrast media, radiopharmaceuticals, and BNCT but also for understanding the mode of action and metabolic characteristics of existing drugs. Our study indicates that laser-SNMS is a sensitive technique for direct imaging of atoms and molecules in tissue with the spatial resolution needed for these purposes. The following points support this conclusion:

An ion beam diameter of 500 nm was sufficient to obtain images with subcellular resolution. An even higher resolution could be achieved by an increase of analysis times.

We were able to correlate the distribution of the atom of interest, in our case, ^{10}B with distinct histologic structures, especially the cell nucleus, by coregistration of the distribution of index molecules/molecular fragments. This spatial correlation offers tremendous potential for the interpretation of biological processes in general and, in the context of our study, for precise evaluation of the biodistribution of candidate drugs.

Other authors have suggested to combine the histologic interpretation of mirror-stained tissue directly neighboring the analyzed sample with information obtained from analytical techniques (e.g.; from high-resolution α-autoradiography in BNCT; refs. 27, 28). These techniques, however, do not allow subcellular spatial resolution. In principle, the approach shown here may also benefit from histologic analysis of mirror-stained slices neighboring the analyzed surface. However, the quality of the stained sections is limited because they have to be fractured off

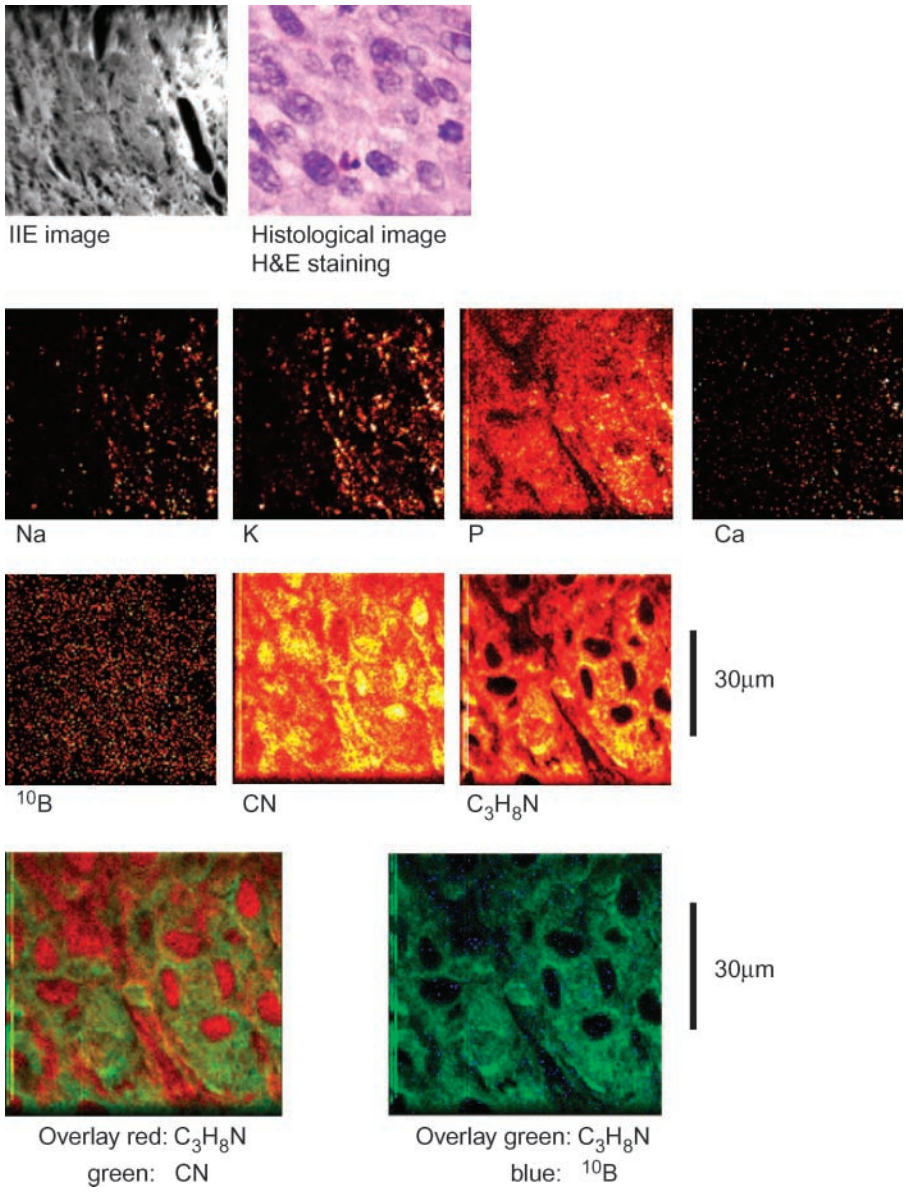

Figure 3. *Row 1,* ion-induced electron image of the surface and histologic image of the tumor (H&E staining) composed mainly of spindle cells. *Rows 2* and *3,* laser-SNMS images of the distribution of Na, K, P, Ca, ^{10}B, CN, and C_3H_8N in a murine sarcoma tumor (xenografted on a nude mouse) after treatment with BSH (200 mg/kg). *Black,* lowest signal intensity; *white,* highest signal intensity. *Row 4,* overlay of the signals from CN and C_3H_8N (*left*) and ^{10}B and C_3H_8N (*right*).

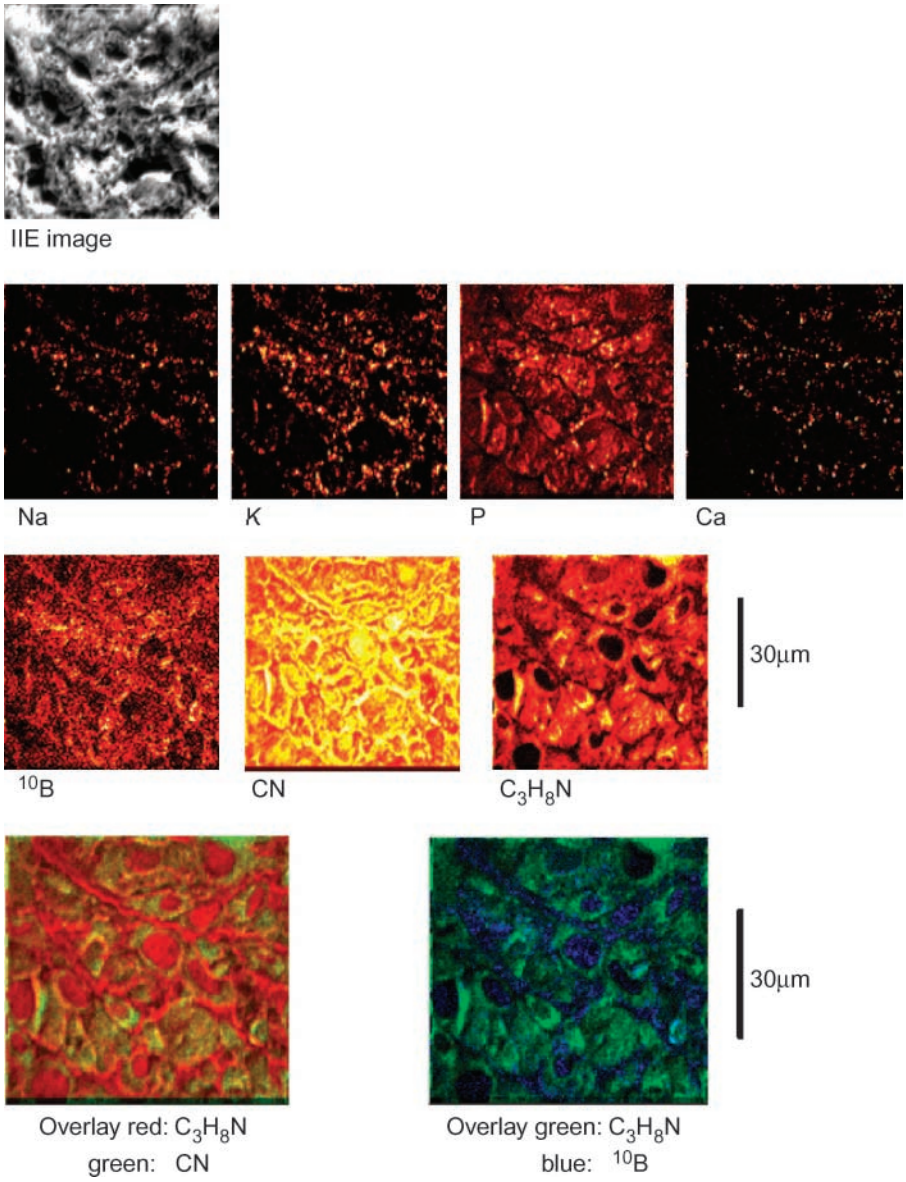

Figure 4. *Row 1,* ion-induced electron image of the sample surface. *Rows 2* and *3,* laser-SNMS images of the distribution of Na, K, P, Ca, ^{10}B, CN, and C_3H_8N in a murine sarcoma tumor (xenografted on a nude mouse) after treatment with BPA (700 mg/kg). *Black,* lowest signal intensity; *white,* highest signal intensity. *Row 4,* overlay of the signals from CN and C_3H_8N (*left*) and ^{10}B and C_3H_8N (*right*).

tissue samples at very low temperatures (143 K; ref. 29) instead of using cutting procedures at higher temperatures (253 K) or resin-embedding procedures. Such conventional fixation and embedding techniques cannot be applied for our purpose because diffusible substances are likely to be redistributed or even lost during sample preparation. Molecular target compounds such as proteins, fatty acids, or drugs might be displaced during fixation.

Laser-SNMS allows for the identification of specific atoms and molecules and the analysis of their distribution in biological samples and therefore has crucial advantageous over other methods such as chemical staining, immunohistochemical tags, and radiolabels, which are common methods for visualizing and identifying molecular targets. Such methods are especially limited with respect to specificity and to the number of target compounds, which can be monitored simultaneously (30). Moreover, use of specific molecular tags requires *a priori* knowledge of the target species, thereby limiting their usefulness for molecular discovery.

SIMS, an alternative technique for element- and molecule-specific imaging, has also been used for imaging boron compounds in cell cultures (31, 32) and tissues (33, 34). However, its application for imaging drugs is substantially hampered due to its lack of sensitivity and accuracy. Laser-SNMS, with the same technical features as SIMS, decouples the sputtering and ionization processes using laser beams to ionize the majority of neutral particles sputtered from the sample surface. The neutral particles yield is less affected by the chemical composition of the surface than the much smaller yield of secondary ions used for SIMS analysis, resulting in a significantly higher sensitivity and

accuracy of laser-SNMS than SIMS. Furthermore, laser-SNMS images are significantly less influenced by topographical effects than SIMS images because the sputtered neutrals are not extracted directly from the surface, as SIMS ions are, but from a defined volume above the surface (35).

Quantification of elements with laser-SNMS has already been shown in cell cultures (23) and was not part of this study.

Laser-SNMS can simultaneously detect elements such as cisplatinum, gadolinium, fluoride, and iodine contained in drugs or molecular fragments of drugs.

The especially developed cryopreparation technique preserves the tissue samples in a state that is close to its natural existence and largely avoids structural artifacts caused by tissue extraction thus minimizing redistribution artifacts for diffusible elements (24).

However, due to the sophisticated preparation and time-consuming measurements, laser-SNMS is not suited as a screening technique in drug development. This can be achieved by use of a complementary technique. In the context of BNCT, the combination of PGRA and laser-SNMS proved to be highly effective.

For this investigation, the concept was to efficiently assess the potential of BSH and BPA in sarcoma. PGRA or alternative methods, such as inductively coupled plasma-atomic emission spectroscopy, can effectively measure the ^{10}B concentration in macroscopic samples to estimate the absolute ^{10}B concentration. Such data can be used to conclude as to whether the amount of boron in a tumor is sufficiently high for treatment and if ^{10}B, as delivered by a specific drug, accumulates in healthy organs revealing organs at risk. This screening method (high throughput)

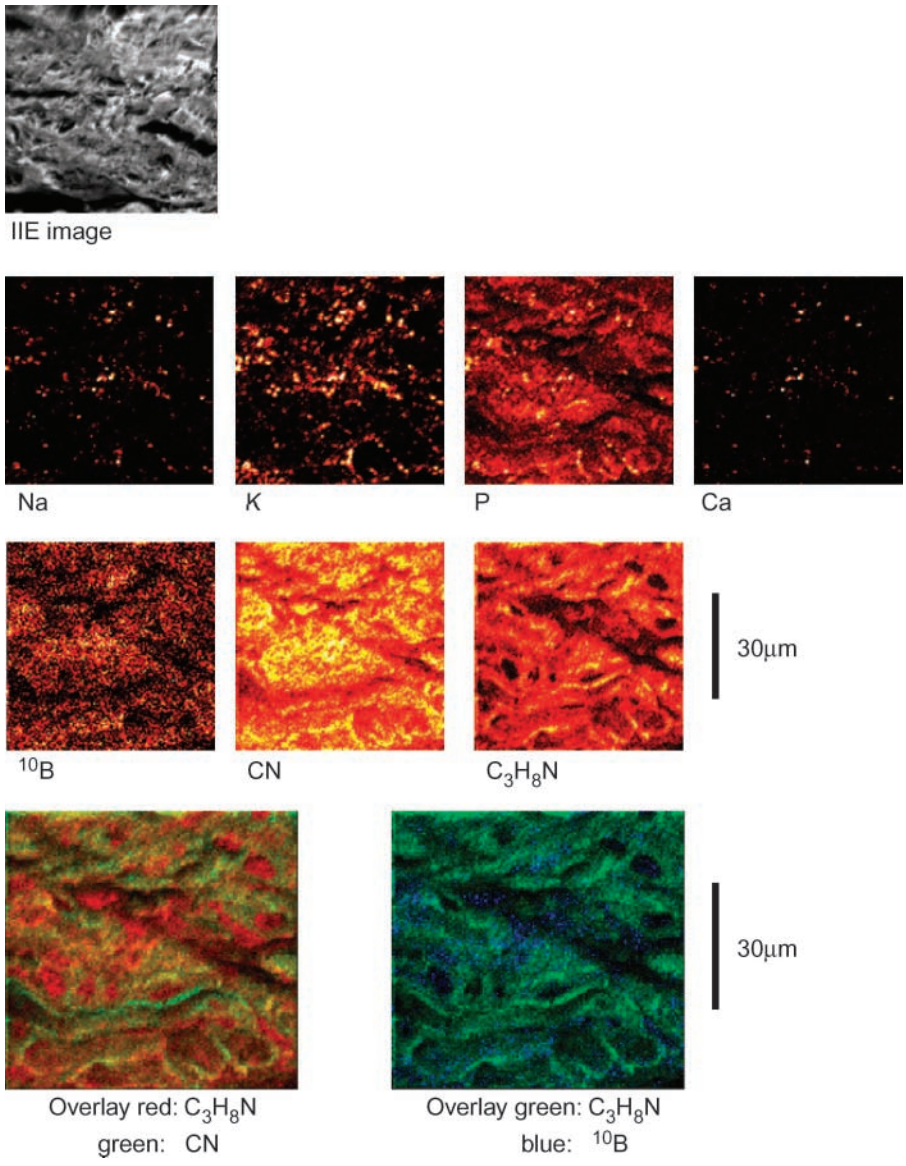

Figure 5. Images of the murine sarcoma MuEs after treatment with BPA and BSH. *Row 1,* ion-induced electron image of the sample surface. *Rows 2* and *3,* laser-SNMS images of the distribution of Na, K, P, Ca, ^{10}B, CN, and C_3H_8N in a murine sarcoma tumor (xenografted on a nude mouse) after treatment with and BSH (200 mg/kg) and BPA (700 mg/kg). *Black,* lowest signal intensity; *white,* highest signal intensity. *Row 4,* overlay of the signals from CN and C_3H_8N (*left*) and ^{10}B and C_3H_8N (*right*).

can ideally be supplemented for promising compounds by laser-SNMS, which can image the ^{10}B distribution with subcellular spatial resolution thus allowing to estimate the effect of boron neutron capture reactions during neutron irradiation. The combination of results from both methods moreover allowed conclusions to be drawn, which are not possible with either technique alone.

In this study, BSH and BPA were applied in the MuEs tumor model. PGRA revealed that BPA might be suitable for a BNCT treatment due to the accumulation of ^{10}B in the tumor compared with blood and all normal tissues investigated. After injection of BSH alone, ^{10}B was not increased in the tumor compared with blood; however, surprisingly, the ^{10}B concentration was found to be higher in the tumor as in healthy organs. The ^{10}B concentration ratio between tumor and muscle was clearly higher as the ratio, which could be achieved with BPA, therefore rendering BSH also an interesting candidate for further testing. Following an observation of Yokoyama et al. (36) and Chandra et al. (32), the sequential injection of BSH and BPA was investigated with the hypothesis that due to the differing uptake mechanisms and pharmacokinetics of these compounds, their combination might enhance the absolute ^{10}B concentration in the tumor, and even more important, it may increase the ^{10}B concentration ratios between tumor and healthy tissue. However, our study showed that the sequential injection of both compounds only increased the absolute ^{10}B concentration in tumor tissue but failed to improve the ^{10}B ratio of the tumor relative to healthy tissues.

This investigation with laser-SNMS was the first study to compare the biodistribution of ^{10}B as delivered by BSH and BPA in tissue samples with a subcellular spatial resolution. It could be shown that both compounds are capable of delivering ^{10}B to the desired target, the cell nucleus, but also to further intracellular compartments. Our study confirmed most assumptions from cell culture experiments by Chandra et al. (32). As opposed to their work, however, within the tumor tissue, we observed a markedly heterogeneous distribution of BPA delivered ^{10}B on both intracellular and intercellular levels. Several mechanisms (differing blood supply, proliferating and metabolic activity, and expression of L-amino acid transporter at the cell membrane) might be responsible for this observation. A heterogeneous microdistribution of ^{10}B has already been postulated by Ono et al. (37) from radiobiological experiments.

Unlike the well-known cellular uptake of BPA by the L-amino acid transport system (38, 39), the uptake mechanism of BSH is still not understood. Due to the almost equal ^{10}B concentrations in tumor tissues and blood, BSH has not been considered as useful to deliver ^{10}B to peripheral tumors, at least not until the combined injection of BSH and BPA was proposed (37) to supposedly reach a more homogeneous ^{10}B distribution. Our results proved that injecting both compounds leads to a more homogenous ^{10}B distribution in the tumor while maintaining the tumor/blood and tumor/healthy tissue ratios at an acceptable level. The combined application of BSH and BPA thus most likely will contribute to an increased efficacy of a BNCT treatment.

With PGRA, we could not prove a significantly improved ratio between tumor and healthy tissues after injection of BSH and BPA compared with BPA alone. However, the favorable ratios after BSH injection alone in muscle and fatty tissue merits further investigation (to optimize the timing of drug delivery for tumors located at the extremities surrounded by muscles and fat). As the ^{10}B concentration in blood and the tumor is equally high, blood vessels have to be regarded as organs at risk. On the other hand, as suggested by Trivillin et al. (40), an impaired function of blood vessels may contribute to the effect of BNCT in the tumor.

We conclude that laser-SNMS is a powerful tool for imaging specific element-containing drugs, which may have tremendous effect on both drug discovery and development. In addition to drug development in BNCT, laser-SNMS may be applied for the development of targeted drugs in oncology, contrast agents, and diagnostic and therapeutic radiopharmaceuticals in nuclear medicine, which all demand precise knowledge of their distribution in tissues and cells.

Disclosure of Potential Conflicts of Interest

No potential conflicts of interest were disclosed.

Acknowledgments

We thank Gero Hilken (Central Animal Facility, University Hospital Essen) and Michael Groneberg (Department of Radiation Oncology, University Hospital Essen) for technical assistance with animal experiments and Klaus Dutschka (Department of Nuclear Medicine, Nuclear Chemistry and Radiopharmaceutics, University Hospital Essen) for help with preparing the compound solutions.

References

1. Arlinghaus HF, Kriegeskotte C, Fartmann M, Wittig A, Sauerwein W, Lipinsky D. Mass spectrometric characterization of elements and molecules in cell cultures and tissues. Appl Surf Sci 2006;252:6941 – 8.

2. Raaijmakers CPJ, Konijnenberg MW, Dewit L, et al. Monitoring of blood-^{10}B concentration for boron neutron capture therapy using prompt γ-ray analysis. Acta Oncol 1995;34:517 – 23.

3. Snyder HR, Reedy AJ, Lennarj WJ. Synthesis of aromatic boronic acids. Aldehyde boronic acids and a boronic acid analog of tyrosine. J Am Chem Soc 1958;80:835 – 8.

4. Soloway AH, Hatanaka H, Davis MA. Penetration of brain and brain tumor. VII. Tumor binding sulfhydryl boron compounds. J Med Chem 1967;10:714 – 7.

5. Nicklas W, Baneux P, Boot R, et al. Recommendations for the health monitoring of rodent and rabbit colonies in breeding and experimental units. Lab Animal 2002;36:20 – 42.

6. Kageji T, Nagahiro S, Mizobuchi Y, Toi H, Nakagawa Y, Kumada H. Boron neutron capture therapy using mixed epithermal and thermal neutron beams in patients with malignant glioma—correlation between radiation dose and radiation injury and clinical outcome. Int J Radiat Oncol Biol Phys 2006;65:1446 – 55.

7. Hatanaka H. A revised boron-neutron capture therapy for malignant brain tumors. II. Interim clinical result with the patients excluding previous treatments. J Neurol 1975;209:81 – 94.

8. Sauerwein W, Zurlo A. The EORTC Boron Neutron Capture Therapy (BNCT) Group: achievements and future projects. Eur J Cancer 2002;38: S31 – 4.

9. Wittig A, Moss RL, Stecher-Rasmussen F, et al. Neutron activation of patients following Boron Neutron Capture Therapy of brain tumors at the High Flux Reactor (HFR) Petten (EORTC Trials 11961 and 11011). Strahlenther Onkol 2005;181:774 – 82.

10. Busse PM, Harling OK, Palmer MR, et al. A critical examination of the results from the Harvard-MIT NCT program phase I clinical trial of neutron capture therapy for intracranial disease. J Neurooncol 2003;62: 111 – 21.

11. Kiger WS, Palmer MR, Riley KJ, Zamenhof RG, Busse PM. A pharmacokinetic model for the concentration of ^{10}B in blood after boronophenylalanine-fructose administration in humans. Radiat Res 2001;155:611 – 8.

12. Bergenheim AT, Capala J, Roslin M, Henriksson R. Distribution of BPA and metabolic assessment in glioblastoma patients during BNCT treatment: a microdialysis study. J Neurooncol 2005;71:287 – 93.

13. Kato I, Ono K, Sakurai Y, et al. Effectiveness of BNCT for recurrent head and neck malignancies. Appl Radiat Isot 2004;61:1069 – 73.

14. Aihara T, Hiratsuka J, Morita N, et al. First clinical case of boron neutron capture therapy for head and neck malignancies using ^{18}F-BPA PET. Head Neck 2006;28:850 – 5.

15. Wittig A, Malago M, Collette L, et al. Uptake of two ^{10}B-compounds in liver metastases of colorectal adenocarcinoma for extracorporeal irradiation with boron neutron capture therapy (EORTC Trial 11001). Int J Cancer 2008;122:1164 – 71.

16. van Rij CM, Sinjewel A, van Loenen AC, et al. Stability of ^{10}B-L-boronophenylalanine-fructose injection. Am J Health Syst Pharm 2005; 62:2608 – 10.

17. Ono K, Masunaga S-I, Suzuki M, Kinashi Y, Takagaki M, Akaboshi M. The combined effect of boronophenylalanine and borocaptate in boron neutron capture therapy for SCCVII tumors in mice. Int J Radiat Oncol Biol Phys 1999;43:431 – 6.

18. Dagrosa MA, Viaggi M, Kreimann E, et al. Selective uptake of *p*-borophenylalanine by undifferentiated thyroid carcinoma for boron neutron capture therapy. Thyroid 2002;12:7 – 12.

19. Masunaga S, Nagasawa H, Hiraoka M, et al. Applicability of the 2-nitroimidazole-sodium borocaptate-^{10}B conjugate, TX-2060, as a ^{10}B-carrier in boron neutron capture therapy. Anticancer Res 2004;24: 2975 – 83.

20. Michel J, Saverwein W, Wittig A, Balossier G, Zierold K. Subcellular localization of boron in cultured melanoma cells by electron energy-loss spectroscopy of freeze-dried cryosections. J Microsc 2003;210:25 – 34.

21. Kriegeskotte C, Möller J, Lipinsky D, et al. Imaging of atomic and molecular species in tissue with laser-SNMS for pharmaceutical studies. Surf Interface Anal 2006;38:121 – 5.

22. Wittig A, Wiemann M, Fartmann M, et al. Preparation of cells cultured on silicon wafers for mass spectrometry analysis. Microsc Res Tech 2005; 66:248 – 58.

23. Fartmann M, Kriegeskotte C, Dambach S, Wittig A, Sauerwein W, Arlinghaus HF. Quantitative imaging of atomic and molecular species in cancer cultures with TOF-SIMS and Laser-SNMS. Appl Surf Sci 2004; 231 – 232:428 – 31.

24. Arlinghaus HF, Fartmann M, Kriegeskotte C, et al. Subcellular imaging of cell cultures and tissue for boron localization with laser-SNMS. Surf Interface Anal 2004;36:698 – 701.

25. Bourdos N, Kollmer F, Benninghoven A, Sieber M, Galla HJ. Imaging of domain structures in a one-component lipid monolayer by time-of-flight secondary ion mass spectrometry. Langmuir 2000;16:1481 – 4.

26. Malmberg P, Nygren HK, Richter K, et al. Imaging of lipids in human adipose tissue by cluster ion TOF-SIMS. Microsc Res Technique 2007;70: 828 – 35.

27. Zamenhof RG, Clement S, Lin K, Lui C, Ziegelmiller D, Harling OK. Monte Carlo treatment planning and high-resolution α-track autoradiography for neutron capture therapy. Strahlenther Onkol 1989;165: 188 – 92.

28. Kiger WS III, Micca PL, Morris GM, Coderre JA. Boron microquantification in oral mucosa and skin following administration of a neutron capture therapy agent. Radiat Prot Dosimetry 2002;99:409 – 12.

29. Echlin P. Low-temperature microscopy and analysis. New York: Plenum Press; 1992.

30. Signor L, Varesio E, Staack RF, Starke V, Richter WF, Hopfgartner G. Analysis of erlotinib and its metabolites in rat tissue sections by MALDI quadrupole time-of-flight mass spectrometry. J Mass Spectrom 2007;42: 900 – 9.

31. Bennett BD, Zha X, Gay I, Morrison GH. Intracellular boron localization and uptake in cell cultures using imaging secondary ion mass spectrometry (ion microscopy) for neutron capture therapy for cancer. Biol Cell 1992; 74:105 – 8.

32. Chandra S, Lorey DRI, Smith DR. Quantitative subcellular secondary ion mass spectrometry (SIMS) imaging of boron-10 and boron-11 isotopes in the same cell delivered by two combined BNCT drugs: *in vitro* studies on human glioblastoma T98G cells. Radiat Res 2002;157:700 – 10.

33. Chandra S, Smith DR, Morrison GH. Subcellular imaging by dynamic SIMS ion microscopy. Anal Chem 2000;72:104A – 14.

34. Yokoyama K, Miyatake S-I, Kajimoto Y, et al. Analysis of boron distribution *in vivo* for boron neutron capture therapy using two different boron compounds by secondary ion mass spectrometry. Radiat Res 2007; 167:102 – 9.

35. Kollmer F, Bourdos N, Kamischke R, Benninghoven A. Nonresonant Laser-SNMS and TOF-SIMS analysis of sub-μm structures. Appl Surf Sci 2003;203:238 – 43.

36. Yokoyama K, Miyatake SI, Kajimoto Y, et al. Pharmacokinetic study of BSH and BPA in simultaneous use for BNCT. J Neurooncol 2006;78: 227 – 32.

37. Ono K, Masunaga SI, Kinashi Y, et al. Radiobiological evidence suggesting heterogeneous microdistribution of boron compounds in tumors: its relation to quiescent cell population and tumor cure in neutron capture therapy. Int J Radiat Oncol Biol Phys 1996;34: 1081 – 86.

38. Wittig A, Sauerwein WA, Coderre JA. Mechanisms of transport of *p*-borono-phenylalanine through the cell membrane *in vitro*. Radiat Res 2000;153:173 – 80.

39. Coderre JA, Glass JD, Fairchild RG, Roy U, Cohen S, Fand I. Selective targeting of boronophenylalanine to melanoma in BALB/c mice for neutron capture therapy. Cancer Res 1987;47:6377 – 83.

40. Trivillin VA, Heber EM, Nigg DW, et al. Therapeutic success of boron neutron capture therapy (BNCT) mediated by a chemically non-selective boron agent in an experimental model of oral cancer: a new paradigm in BNCT radiobiology. Radiat Res 2006;166:387 – 96.